

Fast-Neutron Activation of Long-Lived Isotopes in Enriched Ge

S.R. Elliott,* V.E. Guiseppe,[†] and B.H. LaRoque
Physics Division, Los Alamos National Laboratory, Los Alamos, NM 87545

R.A. Johnson
Department of Physics, University of Washington, Seattle WA, 98195

S.G. Mashnik
X Division, Los Alamos National Laboratory, Los Alamos, NM 87545
(Dated: August 7, 2022)

We measured the production of ^{57}Co , ^{54}Mn , ^{68}Ge , ^{65}Zn , and ^{60}Co in a sample of Ge enriched in isotope 76 due to high-energy neutron interactions. These isotopes are critical in understanding background in Ge detectors used for double-beta decay experiments. These isotopes are produced by cosmogenic-neutron interactions in the detectors while they reside on the Earth's surface. We compared the measured production to that predicted by cross-section calculations based on CEM03.02. The cross section calculations over-predict our measurements by approximately a factor of two depending on isotope. We then use the measured cosmic-ray neutron flux and our results to predict the cosmogenic production rate with an accuracy near 15%.

PACS numbers: 23.40.-s, 25.40.Fq, 25.40.Sc

I. INTRODUCTION

Neutrinoless double-beta decay ($0\nu\beta\beta$) plays a key role in understanding the neutrino's absolute mass scale and particle-antiparticle nature [1, 2, 3, 4, 5, 6]. If this nuclear decay process exists, one would observe a mono-energetic line originating from a material containing an isotope subject to this decay mode. One such isotope that may undergo this decay is ^{76}Ge . Germanium-diode detectors fabricated from material enriched in ^{76}Ge have established the best half-life limits and the most restrictive constraints on the effective Majorana mass for the neutrino [7, 8]. One analysis [9] of the data in Ref. [8] claims evidence for the decay with a half-life of $2.23_{-0.31}^{+0.44} \times 10^{25}$ y. Planned Ge-based $0\nu\beta\beta$ experiments, MAJORANA [10, 11, 12] and GERDA [13], will test this claim. Eventually, these future experiments target a sensitivity of $>10^{27}$ y or ~ 1 event/ton-year to explore neutrino mass values near that indicated by the atmospheric neutrino oscillation results.

The key to these experiments lies in the ability to reduce intrinsic radioactive background to unprecedented levels and to adequately shield the detectors from external sources of radioactivity. Previous experiments' limiting backgrounds have been trace levels of natural decay chain isotopes within the detector and shielding components. The γ -ray emissions from these isotopes can deposit energy in the Ge detectors producing a continuum, which may overwhelm the potential $0\nu\beta\beta$ signal peak at 2039 keV. Great progress has been made in

identifying the location and origin of this contamination, and future efforts will substantially reduce this contribution to the background. The background level goal of 1 event/ton-year, however, is an ambitious factor of ~ 400 improvement over the currently best achieved background level [8]. If the efforts to reduce the natural decay chain isotopes are successful, previously unimportant components of the background must be understood and eliminated. The contribution from long-lived isotopes produced by cosmic-ray neutrons in Ge detectors fabricated from enriched Ge was recognized and described in [14, 15]. In fact, the dominant background that the MAJORANA and GERDA experiments will face, without sophisticated analysis cuts, will originate from such isotopes unless mitigation strategies to reduce the activation are successful.

To successfully mitigate the impact of these isotopes requires an understanding of their production. Tables I and II summarize the previous production rate estimates. The two most critical cosmogenic isotopes, ^{60}Co and especially ^{68}Ge , show significant variation in the predicted rates: factors of ≈ 2 and ≈ 10 respectively. For ^{60}Co , some models predict a higher production rate for enriched Ge ($^{\text{enr}}\text{Ge}$) than for Ge samples with natural isotopic content ($^{\text{nat}}\text{Ge}$). Reference [16] gives a nice summary of previous attempts to calculate the production rates of the problematic isotopes, and provides an estimate of its own. The authors of that report noted that the calculations differ significantly and that measurements would be useful to better understand the rates. Some measurements do exist, but are either for proton reactions [17, 18, 19], or have a large uncertainty [15]. Since the production rates due to neutrons are much larger than for protons, it's important to have neutron reaction measurements. In addition, Barabanov *et al.* [20] studied the reduction of cosmogenic activation as it depends on shielding in order

*elliotts@lanl.gov

[†]Present address: University of South Dakota, Vermillion, SD 57069

TABLE I: A summary of previous estimates of the production of long-lived cosmogenic isotopes in $^{\text{nat}}\text{Ge}$ for the isotopes studied in this work. The production rates are given in atoms/(kg d). The data in Ref. [26] was quoted in $\mu\text{Bq/kg}$ and we converted to units presented.

Isotope	Ref. [14]	Ref. [15] (Calc.)	Ref. [15] (Expt.)	Ref. [26]	Ref. [20]	Ref. [16]	Ref. [22]	Ref. [21]
^{57}Co	0.5	4.4	2.9 ± 0.4	10.2		9.7	6.7	13.5
^{54}Mn		2.7	3.3 ± 0.8	9.1		7.2		2.7
^{68}Ge	26.5	29.6	30 ± 7	58.4	82.8	89	45.8	41.3
^{65}Zn	30.0	34.4	38 ± 6	79.0		77	29.0	37.1
^{60}Co	4.8			6.6	2.9	4.8	2.8	2.0

to design an optimum transport container. That reference also calculated the rates for cosmic-ray proton reactions and found the production rates for the troublesome isotopes to be about a factor of 10 below that for cosmic-ray neutrons. The work of Mei *et al.* [21] noted that much of the large variation in these rates was due to the use of different cosmic ray neutron flux estimates, and that many of the analyses ([14, 15, 20, 22]) used historical flux spectra that are less precise than modern measurements. Although Ref. [21] performed calculations for the production of the isotopes of interest to this paper, the cross sections were calculated using TALYS [23]. This code only predicts cross sections to an energy of 250 MeV, whereas other treatments go to higher energies. Reference [16] used a modern interpretation of the old neutron flux values [24] but not the results of recent measurements [25]. Furthermore, it used a combination of cross section calculations in order to span the energies necessary for the calculations. Reference [26] presented numbers for a specific shielding geometry, which is not easy to translate to a raw production rate with the provided data. Hence none of the presently available estimates are sufficient to reliably predict the cosmogenic production rates and new measurements/estimates are required.

We exposed a sample of Ge enriched in isotope 76 to a wide-band neutron beam that resembles the cosmic-ray neutron flux. After exposure we counted the sample in a low-background counting system to observe the γ rays from the decays of the problematic isotopes. From these data we have measured the production rate due to fast neutrons in a Ge sample enriched in isotope 76 that was taken from material used for Ge detector production. With knowledge of the neutron-beam and cosmic-neutron energy spectra, we used these data to provide an estimate of the production rate due to exposure of Ge to cosmic rays. We used a cross-section calculation that spans the energy range of interest and the most recent cosmic-ray neutron flux measurements of which we are aware. This article describes our determination of values for the production rate of these isotopes.

TABLE II: A summary of previous estimates of the production of long-live cosmogenic isotopes in $^{\text{enr}}\text{Ge}$ for the isotopes studied in this work. For these estimates, the abundance values are 14% for ^{74}Ge , 86% for ^{76}Ge and zero for the other naturally occurring isotopes. The production rates are given in atoms/(kg d).

Isotope	Ref. [14]	Ref. [15]	Ref. [20]	Ref. [16]	Ref. [22]	Ref. [21]	This Work
^{57}Co	0.1	1.0		2.3	2.9	6.7	1.2 ± 0.2
^{54}Mn		1.4		5.4	2.2	0.87	2.0 ± 0.3
^{68}Ge	1.2	1.2	5.7	13	7.6	7.2	2.1 ± 0.3
^{65}Zn	6.0	6.4		24	10.4	20.0	8.9 ± 1.2
^{60}Co	3.5		3.3	6.7	2.4	1.6	2.5 ± 0.4

II. EXPERIMENT

The sample was exposed to the neutron beam at the Los Alamos Neutron Science Center (LANSCE) Weapons Neutron Research (WNR) facility from Target 4 Flight Path 60 Right (4FP60R) [27]. As the broad-spectrum, pulsed neutron beam strikes the Ge target, the outgoing γ rays are detected by the GERmanium Array for Neutron Induced Excitations (GEANIE) spectrometer [28]. The corresponding data from the GEANIE spectrometer will be used for $(n,n'\gamma)$ analysis that will be presented in a separate publication. The GEANIE sample is located a distance of 20.34 m from the natural tungsten spallation target.

The target sample was a 11.13-gm, 22-mm diameter metal enriched Ge ($^{\text{enr}}\text{Ge}$) powder contained within a plastic enclosure. The isotopic abundances within the sample were measured by time of flight secondary ion mass Spectrometry (ToF SIMS) with the result: ^{70}Ge $0.77\pm 0.04\%$, ^{72}Ge $0.94\pm 0.05\%$, ^{73}Ge $0.36\pm 0.03\%$, ^{74}Ge $13.81\pm 0.18\%$, and ^{76}Ge $84.12\pm 0.23\%$. The sample was exposed with two separate beam collimations (3/4" and 1/2" collimators) during 3 irradiation periods. For the 3/4"-collimator (1/2"-collimator) run a surface area of 2.85 (1.27) cm^2 was exposed to the beam. The 3/4"-collimator exposure was performed between July 16 and July 23, 2007 (6.99 d elapsed time). The 1/2"-collimator exposure was performed between July 27 and August 2, 2007 (5.95 d) and then between August 8 and August 14, 2007 (6.19 d). As seen in Fig. 1, the energy spectrum of the third exposure was slightly softer than the other 2 exposures at the higher energies. The pulsed neutron beam has the following timing structure. Macropulses, lasting 625 μs , occur at a rate of 40 Hz. Micropulses are spaced every 1.8 μs , during which the neutron energy is determined by the time of flight from the micropulse start. An in-beam fission chamber measures the neutron flux with ^{238}U foils.

The powder was stored for an extended period and therefore any radioactivity had decayed to an extremely low level (<150 Bq) before counting began. Therefore, this sample was well below any action levels and not subject to any source-handling requirements. The sample

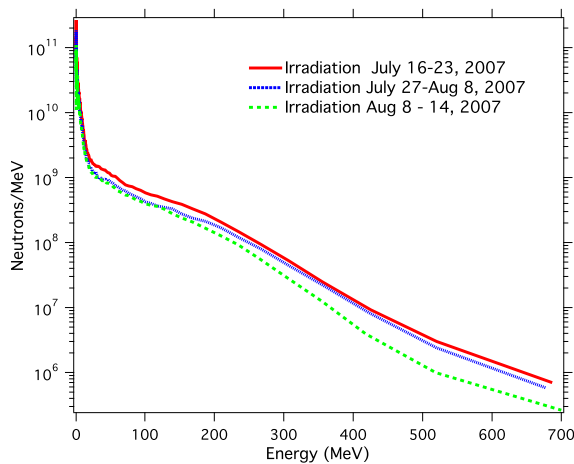


FIG. 1: The energy spectrum for the neutron beam fluence at 4FP60R for the 3 separate exposure periods. The data are corrected for live time of the fission chamber.

was transported to our low-background counting facility underground at the Waste Isolation Pilot Plant (WIPP) near Carlsbad, NM and counted with a Ge detector. The detector was fabricated in 1985 and placed underground at WIPP in 1998. It is an n-type semi-coax design with a height of 41 mm and a diameter of 51 mm. It is contained within an ≈ 1 -mm thick Cu cryostat. The shield during these runs consisted of 5 cm of oxygen-free, high-conductivity Cu and 10 cm of Pb.

The sample was counted over a period of 73.86 days between February 19 and May 4, 2009 with a total live time of 49.02 days. The spectrum is shown in Fig. 2. The detector at WIPP has been underground there for over 10 years and therefore any activities of isotopes of interest to this study, that may have been produced while that detector was exposed to cosmic rays as it resided on the Earth's surface, have long since decayed away. The lone exception to this is a very low level of ^{60}Co that resides in the Cu cryostat of the Ge detector and the inner layer of the shield that is also Cu. The background spectrum in Fig. 2 shows that this rate is very small compared to the sample's ^{60}Co rate. The data presented in Table III includes a subtraction of this background ($\approx 10\%$) for the ^{60}Co count rates.

III. MEASURED PRODUCTION RATES

The peaks in Fig. 2 were fit to determine the measured counts (C) and the results are given in Table III. The efficiency for counting the γ rays in the geometry used for the sample was determined by using $^{57,60}\text{Co}$, ^{54}Mn , ^{22}Na and ^{137}Cs sources. The geometry of these sources is coincidentally very similar to the Ge sample and therefore there was no need for simulation to determine the efficiencies. These sources had calibrated activities known to $\pm 1\%$. Since many of the lines of interest come from

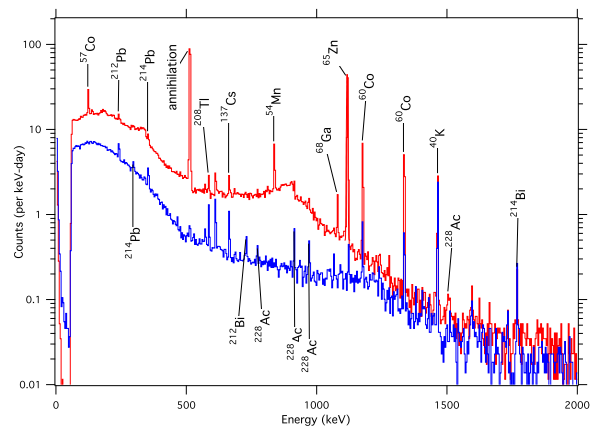


FIG. 2: The energy spectrum of γ rays from the $^{\text{enr}}\text{Ge}$ sample as measured by a Ge detector (upper curve). Also shown is a background spectrum taken with no sample present. (lower curve)

these isotopes, the measurements were a direct calibration of the efficiencies of interest. For ^{65}Zn and ^{68}Ga lines, a γ -ray efficiency curve was determined from the various lines in these sources in order to interpolate between the measured line energies. Corrections for summing of coincident transitions and annihilation γ rays within the sources were made. The resulting efficiencies and their uncertainty resulting from counting statistics and the interpolation and summing corrections are given in Table III. For the ^{60}Co calibration, a high event rate resulted in a minor peak distortion that the other data sets did not suffer. We took an additional uncertainty for those peaks to reflect that. We used a random pulser to verify the event-rate dependence of the data-acquisition system dead time.

In addition to the γ -ray detection efficiency (ϵ_γ), an efficiency factor must also be included to take into account the decay of the isotope since the end of exposure and during the counting period. This latter efficiency factor (ϵ_c) depends on the half-life of the isotope of interest and is also given in Table III.

With these efficiencies, it is straight-forward to calculate the number of atoms of each isotope that were present at the end of exposure to neutrons (August 14, 2007). The measured number of atoms at the reference date of the end of exposure (N_0) is given by:

$$N_0 = \frac{C}{\epsilon_\gamma \epsilon_c B}, \quad (1)$$

where

$$\epsilon_c = \sum_i (e^{-\lambda T_{start}^i} - e^{-\lambda T_{end}^i}), \quad (2)$$

and T_{end}^i (T_{start}^i) is the number of days since the end of exposure that the counting stopped (started) for each

of the i data runs, λ is the decay rate of the isotope in question, B is the fraction of decays that emit the γ ray of interest.

The predicted number of atoms N_0^{Pred} can also be expressed in terms of the reaction rates during the 3 exposure periods:

$$N_0^{Pred} = \sum_i \frac{k_i}{\lambda} (1 - e^{-\lambda T_{irrad}^i}) e^{-\lambda T_{decay}^i} \quad (3)$$

where we have corrected for the decay during the exposure and the decay after the exposure until the reference date. In Eqn. 3, T_{irrad}^i is the duration time of irradiation of the i^{th} exposure, and T_{decay}^i is the time between the end of exposure i and the reference date for N_0 . k_i is the production rate (atoms/day) during exposure i and is given by:

$$\begin{aligned} k_i &= \frac{n_s}{t_i} \int F_i(E) \sigma(E) dE \\ &= \left(\frac{M_s N_A}{(MW) A t_i} \right) f_i \end{aligned} \quad (4)$$

where n_s is the number of exposed sample nuclei per unit area in exposure i of duration t_i , $F_i(E)$ is the energy (E) dependent neutron fluence (number of neutrons per MeV) impinging upon the sample during exposure i and $\sigma(E)$ is the energy dependent cross section calculated for our sample and its measured isotopic abundances. f_i is the fluence and cross section energy-dependent integral for each exposure. Since the beam spot on the sample is smaller than the sample, n_s can be related to the total sample mass (M_s , 11.13 g) and the sample area (A , 3.80 cm²). The beam spot is rather large compared to the sample geometry, however, and therefore we have ignored any uncertainty associated with non-uniformities of the source. That is, any such non-uniformities will average to the source nominal area density.

N_0^{Pred} can be written:

$$N_0^{Pred} = \frac{M_s N_A}{(MW) \lambda A} \sum_i f_i (1 - e^{-\lambda T_{irrad}^i}) e^{-\lambda T_{decay}^i} \quad (5)$$

where N_A is Avagadro's number, and MW is the molecular weight (75.62 for our sample).

A number of systematic effects add to the uncertainty in N_0 . These include the uncertainty in the nuclear physics parameters, which come from the National Nuclear Data Center. The values for the half-lives and branching ratios are known to high precision and are a negligible contribution to the total uncertainty. The uncertainty in ϵ_γ is described above and included in the quoted values. However, each of the sources have an additional uncertainty due to the precision of the known activity of 1%. The start and stop times of counting and the live time of the counting are known to a small percentage and are negligible contributions to the uncertainty.

This is similar for the times associated with the irradiation. The sample had been stored on the Earth's surface for many years prior to exposure to the beam and then counting at WIPP. Any isotopes produced by cosmic ray neutrons would certainly be at saturation after this extended period. The saturation production rates however are predicted to be near 1 atom/(day kg). Therefore the total count rate for our 11 g sample due to this contribution is several orders of magnitude less than our measured count rate and we ignore this systematic effect.

IV. CROSS SECTIONS

If the energy dependence of the neutron fluence over the duration of the exposure had been constant and identical in shape to the cosmic-ray neutron flux, we could have used a simple neutron-flux scaling between our measurements and the cosmic-neutron flux to estimate the cosmogenic production of these isotopes. Since the shapes do differ slightly, we used a model for the cross section to adjust for these spectral differences in order to make a prediction regarding the cosmic-ray production rates. For this purpose, we use cross sections for isotope production calculated using Cascade-Exciton Model (CEM03.02 [29, 30, 31]) as it usually has a better predictive power in comparison with other similar available models (see, e.g. [32]). The CEM formalism permits the calculation of cross sections to the high energies necessary for this work. We assumed that the energy dependence of the cross section is correct but that there may be an overall normalization uncertainty. This procedure then corrects for any normalization uncertainty.

To determine the yield of an isotope, one must consider all feeder isotopes that may decay to the isotope of interest. Therefore to determine the cumulative cross section for ⁵⁷Co for example, one must sum the cross sections for ⁵⁷Co, ⁵⁷Ni, ⁵⁷Cu and ⁵⁷Zn. Similarly for ⁶⁸Ge, one must also consider ⁶⁸As and for ⁶⁵Zn one must consider ⁶⁵Zn, ⁶⁵Ga, ⁶⁵Ge and ⁶⁵As. For the isotopes ⁵⁴Mn and ⁶⁰Co one only need consider the primary isotopes. Note, that for the case of ⁶⁰Co, this is only approximately true. Because of the long half-life of ⁶⁰Fe, the contributions of ⁶⁰Fe, ⁶⁰Mn and ⁶⁰Cr are negligible. Using the CEM3.02 code, Tables IV through VIII provide the values of these cumulative cross sections summed over the feeders for the 5 isotopes that comprise Ge.

Note that Fig. 3 indicates that the production rates of the isotopes of interest are dominated by neutron energies between about 100 and 750 MeV. This is the energy region for which 4FP60R has appreciable neutron flux and it is a good comparison beam for the cosmogenic production.

TABLE III: A summary of N_0 for the long-lived isotopes in the ^{enr}Ge sample. The uncertainty quoted for N_0 is statistical and arises only from the counting statistics of the measured peaks. The quoted uncertainty for N_0^{Pred} arises from the uncertainty in the 4FP60R neutron fluence. Systematic uncertainties are summarized in Table X and discussed in the text.

Isotope	$\tau_{1/2}$ (days)	γ -ray Energy	C	ϵ_γ	ϵ_c	B	N_0	N_0^{Pred}
^{57}Co	271.8	122.1 keV	2916±84	0.1663(7)	0.0280	0.856	$7.31 \pm 0.21 \times 10^5$	$1.73 \pm 0.06 \times 10^6$
^{57}Co	271.8	136.5 keV	386±63	0.163(2)	0.0280	0.107	$7.89 \pm 1.3 \times 10^5$	$1.73 \pm 0.06 \times 10^6$
^{54}Mn	312.1	834.9 keV	1084±43	0.0302(3)	0.0297	1.000	$1.21 \pm 0.05 \times 10^6$	$1.79 \pm 0.05 \times 10^6$
^{68}Ge	270.8	1077.4 keV	198±18	0.0207(5)	0.0280	0.032	$1.06 \pm 0.10 \times 10^7$	$2.92 \pm 0.02 \times 10^7$
^{65}Zn	244.25	1115.5 keV	8541±95	0.0232(5)	0.0262	0.506	$2.77 \pm 0.03 \times 10^7$	$5.03 \pm 0.06 \times 10^7$
^{60}Co	1923.6	1173.2 keV	1342±42	0.0200(6)	0.0146	0.999	$4.61 \pm 0.14 \times 10^6$	$7.50 \pm 0.01 \times 10^6$
^{60}Co	1923.6	1332.5 keV	1176±39	0.0167(3)	0.0146	1.000	$4.83 \pm 0.16 \times 10^6$	$7.50 \pm 0.01 \times 10^6$

TABLE IV: The calculated cumulative cross sections for production of selected cosmogenic isotopes in ^{70}Ge . The cross sections are cumulative because they are sums over all isotopes that feed the isotope of interest.

Energy (MeV)	Isotope Production Cross Section (mb)				
	^{57}Co	^{54}Mn	^{68}Ge	^{65}Zn	^{60}Co
10	0	0	0	0	0
20	0	0	0	0	0
30	0	0	295.6	16.63	0
40	0	0	248.0	97.52	0
50	0	0	153.1	51.05	0.0022
60	0	0	119.6	36.86	0.034
70	0	0	101.6	55.99	0.53
80	0.009	0.001	90.53	86.66	0.80
90	0.019	0.0019	82.67	91.14	0.70
100	0.16	0.0037	75.15	88.94	0.80
200	11.49	3.06	50.42	54.34	4.78
300	16.52	7.72	43.50	47.17	4.34
400	18.97	10.59	38.13	41.63	4.38
500	20.34	12.86	33.34	37.14	4.36
600	20.28	14.31	29.17	33.39	4.21
700	19.09	14.49	26.46	30.89	3.81
800	18.59	14.15	24.75	28.58	3.63
900	17.28	13.59	23.36	27.026	3.34
1000	16.27	13.08	22.07	25.99	3.11
2000	10.22	8.12	16.62	20.61	2.17

TABLE V: The calculated cumulative cross sections for production of selected cosmogenic isotopes in ^{72}Ge . The cross sections are cumulative because they are sums over all isotopes that feed the isotope of interest.

Energy (MeV)	Isotope Production Cross Section (mb)				
	^{57}Co	^{54}Mn	^{68}Ge	^{65}Zn	^{60}Co
0	0	0	0	0	0
0	0	0	0	0	0
0	0	0	0	0	0
0	0	0	0	0	0
0	0	0	15.82	0.15	0
0	0	0	45.86	13.43	0
0	0	0	42.57	20.87	0.0010
0	0	0	34.56	18.01	0.014
0	0	0	32.2	19.43	0.20
0	0	0	30.69	30.27	0.61
4.17	4.32	0.99	22.9	42.50	5.26
9.45	10.00	5.03	19.88	38.31	5.78
12.06	12.86	8.55	16.91	34.84	6.22
14.25	15.12	11.47	14.77	31.37	6.56
15.13	16.05	13.91	13.46	28.30	6.45
14.97	15.95	14.48	12.45	25.54	6.09
14.29	15.22	14.62	11.54	23.63	5.85
13.46	14.37	14.54	11.13	21.75	5.52
12.62	13.45	14.07	10.65	20.59	5.14
7.72	8.24	8.79	7.96	14.69	3.27

V. CONVERTING THE MEASURED PRODUCTION RATES TO COSMOGENIC PRODUCTION RATES

To estimate the production rate due to cosmic-ray neutrons, one must know the energy dependent flux of the neutrons and the cross sections.

Ziegler carried out a comprehensive study on the cosmic-ray neutron flux [24] and pointed out that some of the data from early measurements is incorrect or of marginal quality. Mei *et al.* [21] recognized that previous estimates of the cosmogenic production rates used various outdated estimates of the cosmic neutron flux. Improved recent measurements by Gordon *et al.* [25] show that the flux density spectrum at sea level can be parameterized as

$$\phi(E) = 1.006 \times 10^{-6} e^{-0.35 \ln^2 E + 2.1451 \ln E}$$

$$+ 1.011 \times 10^{-3} e^{-0.4106 \ln^2 E - 0.667 \ln E} \quad (6)$$

where E is neutron kinetic energy in MeV and ϕ is given in units of $\text{cm}^{-2}\text{s}^{-1}\text{MeV}^{-1}$. This parameterization function agrees with the data within $\sim 2\%$. Note that parameterization used by Ref. [16] based on that from Ref. [24] differs from that of Ref. [25]. Both curves are shown in Fig. 4.

Gordon's measurements show that the shape of the outdoor ground-level neutron spectrum does not depend significantly on altitude, cutoff or solar modulation. Factors depending on atmospheric depth, geomagnetic cutoff, rigidity, and geomagnetic location are given by Gordon for correcting the flux for these effects. His model is slightly different than Ziegler or the JEDEC standard. As a comparison, the cosmic production rates resulting from Gordon's flux are 13-33% higher than that using the flux of Ziegler for the isotopes of interest in this work.

TABLE VI: The calculated cumulative cross sections for production of selected cosmogenic isotopes in ^{73}Ge . The cross sections are cumulative because they are sums over all isotopes that feed the isotope of interest.

Energy (MeV)	Isotope Production Cross Section (mb)				
	^{57}Co	^{54}Mn	^{68}Ge	^{65}Zn	^{60}Co
10	0	0	0	0	0
20	0	0	0	0	0
30	0	0	0	0	0
40	0	0	0	0	0
50	0	0	0	0	0
60	0	0	4.79	0.08	0
70	0	0	22.14	6.67	0
80	0	0	23.51	13.28	0.002
90	0	0	19.93	11.61	0.017
100	0	0	18.37	12.60	0.13
200	3.63	0.52	15.22	35.05	4.94
300	7.45	3.87	14.00	33.30	6.14
400	10.40	7.34	11.98	30.62	6.88
500	12.84	10.60	10.39	27.92	7.32
600	14.07	13.07	9.20	25.63	7.37
700	13.83	14.45	8.41	23.38	7.17
800	13.67	14.57	7.84	21.48	6.91
900	13.06	14.49	7.25	19.88	6.51
1000	12.51	13.81	6.92	18.58	6.19
2000	7.73	8.64	5.53	12.96	3.94

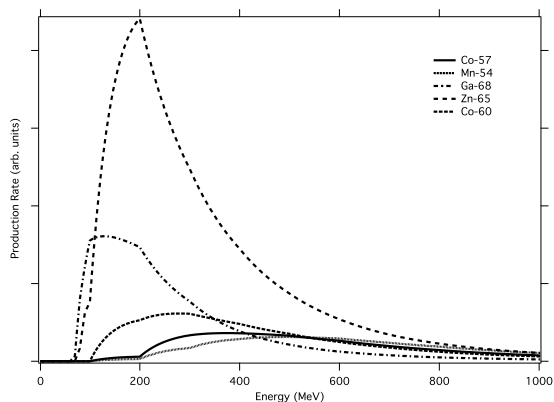


FIG. 3: The CEM cross sections folded with the cosmic-ray neutron energy spectrum as a function of energy for the isotopes of interest.

The ratio of N_0 to N_0^{Pred} values given in Table III can be used to scale a predicted production rate (K_{Gordon}) based on the cross sections of Section IV and the Gordon neutron flux parameterization to provide an estimate (K_{scaled}) of the cosmogenic production rate indicated by our measurements. The numbers used in this arithmetic are summarized in Table IX with the results also quoted in Table II for comparison to previous predictions.

The estimate of the cosmogenic production from these measured results have some additional systematic uncertainties. These include the precision to which the cosmic ray neutron flux is known (10-15% and so we split the difference and use 12.5% [25]). The total cosmogenic

TABLE VII: The calculated cumulative cross sections for production of selected cosmogenic isotopes in ^{74}Ge . The cross sections are cumulative because they are sums over all isotopes that feed the isotope of interest.

Energy (MeV)	Isotope Production Cross Section (mb)				
	^{57}Co	^{54}Mn	^{68}Ge	^{65}Zn	^{60}Co
10	0.00	0.00	0.00	0.00	0.00
20	0.00	0.00	0.00	0.00	0.00
30	0.00	0.00	0.00	0.00	0.00
40	0.00	0.00	0.00	0.00	0.00
50	0.00	0.00	0.00	0.00	0.00
60	0.00	0.00	0.00	0.00	0.00
70	0.00	0.00	0.57	0.00	0.00
80	0.00	0.00	7.78	1.61	0.00
90	0.00	0.00	13.04	6.79	0.00
100	0.00	0.00	12.79	8.06	0.01
200	1.03	0.23	10.76	28.71	4.07
300	5.37	2.73	10.43	28.24	6.04
400	8.16	6.14	8.74	27.13	7.28
500	10.85	9.52	7.69	25.33	8.09
600	12.16	12.18	6.85	23.42	8.08
700	12.77	13.66	6.17	21.17	8.19
800	12.40	14.34	5.44	19.32	7.64
900	11.96	14.44	5.11	17.64	7.32
1000	11.36	13.93	4.78	16.47	6.88
2000	7.03	8.76	3.79	11.31	4.46

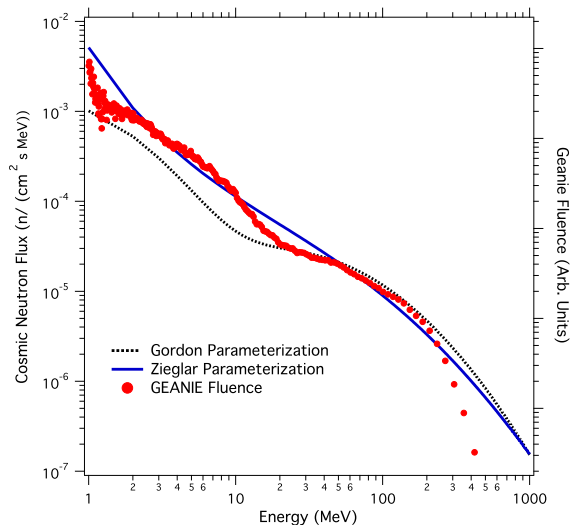


FIG. 4: The measured neutron flux parameterization functions at sea level [24, 25] and a normalized plot of the 4FP60R neutron fluence showing that the spectral shape in the critical 100-300 MeV range is similar to the cosmic ray spectrum.

rate includes contributions from subdominant proton and pion interactions. These only contribute approximately 10% [20] to the total production rate. These charged particles are much less penetrating than neutrons and therefore their impact on any given sample is very geometry dependent. Hence we assume a 50% uncertainty on this correction for an uncertainty of 5%. Again these uncertainties are uncorrelated and result in an estimated

TABLE VIII: The calculated cumulative cross sections for production of selected cosmogenic isotopes in ^{76}Ge . The cross sections are cumulative because they are sums over all isotopes that feed the isotope of interest.

Energy (MeV)	Isotope Production Cross Section (mb)				
	^{57}Co	^{54}Mn	^{68}Ge	^{65}Zn	^{60}Co
10	0.00	0.00	0.00	0.00	0.00
20	0.00	0.00	0.00	0.00	0.00
30	0.00	0.00	0.00	0.00	0.00
40	0.00	0.00	0.00	0.00	0.00
50	0.00	0.00	0.00	0.00	0.00
60	0.00	0.00	0.00	0.00	0.00
70	0.00	0.00	0.00	0.00	0.00
80	0.00	0.00	0.00	0.00	0.00
90	0.00	0.00	0.04	0.00	0.00
100	0.00	0.00	1.00	0.19	0.00
200	0.12	0.11	5.52	17.18	1.95
300	2.43	1.24	5.92	19.91	5.07
400	4.92	3.94	5.27	20.67	7.15
500	7.39	7.15	4.69	20.14	8.52
600	9.16	10.34	4.11	18.97	9.12
700	9.84	12.25	3.73	17.41	9.40
800	10.21	13.63	3.36	16.11	9.16
900	10.02	13.86	3.08	14.84	8.66
1000	9.62	14.00	2.85	13.60	8.36
2000	5.82	8.92	1.82	8.67	5.43

TABLE IX: A summary of the parameters that enter into the calculation of our estimate for the cosmic-ray production rate of the various isotopes (K_{scaled}). The uncertainties quoted for K_{scaled} are explained in Table X. The value for ^{57}Co is taken as that of the 122-keV line as it has a much smaller total uncertainty. The ^{60}Co value is the average of the two individual measurements and, since the uncertainty is dominated by systematic effects, we quote the larger of the two associated total uncertainty values given in Table X.

Isotope	Ratio ($\frac{N_0}{N_{Preed}}$)	K_{Gordon} (atoms/(kg d))	K_{scaled} (atoms/(kg d))
^{57}Co	0.42 ± 0.01	2.93	1.24 ± 0.17
^{54}Mn	0.67 ± 0.03	2.91	1.96 ± 0.28
^{68}Ge	0.36 ± 0.03	5.83	2.12 ± 0.35
^{65}Zn	0.55 ± 0.01	16.24	8.94 ± 1.23
^{60}Co	0.63 ± 0.03	4.06	2.55 ± 0.30

systematic uncertainty of 13.5%. In addition, we have assumed that any uncertainty in the scaling due to the energy dependence of the calculated cross section is small and mostly cancels in the scaling ratio. Any uncertainty in the overall magnitude of the cross section would cancel in the scaling ratio.

We estimated the rate of cosmogenic production is ^{enr}Ge with isotopic abundance limited to isotopes 74 (14%) and 76 (86%). However, a small admixture of isotope 70 can result in significantly more ^{68}Ge due to the much lower threshold for the neutron reaction and the higher cross section. Here we present a rough formula to estimate the ^{68}Ge production rate (P_{68}) as a function

of the amount of ^{70}Ge present in the sample in per cent (X).

$$P_{68} = (2.12 + 0.75X)atoms/kg - d \quad (7)$$

This formula should be accurate to approximately 20%. The other critical isotope for $\beta\beta$ research is ^{60}Co and it has a small production dependence on the fraction of ^{70}Ge .

VI. DISCUSSION AND CONCLUSION

We measured the production of ^{57}Co , ^{54}Mn , ^{68}Ge , ^{65}Zn , and ^{60}Co in a sample of Ge enriched in isotope 76 due to high-energy neutron interactions within a neutron beam with a spectrum similar to that of the cosmic-ray neutron flux at the Earth's surface. The results, presented in Table IX, were compared to cross sections calculated with CEM03.02. The measurements are smaller by about a factor of 2 than these calculations depending on isotope. Our estimated total uncertainty for the production rates is approximately 20% providing much better guidance to double-beta decay experimenters in their efforts to understand background due to these isotopes.

Acknowledgments

We gratefully acknowledge the support of the U.S. Department of Energy through the LANL/LDRD Program for this work. We thank Frank Avignone III for providing the enriched Ge sample and we thank Jason Detwiler for a careful reading of this manuscript. This work benefited from the use of the Los Alamos Neutron Science Center, funded by the U.S. Department of Energy under contract DE-AC52-06NA25396. We are grateful for the ToF SIMS measurements that were performed by Zihua Zhu using EMSL, a national scientific user facility sponsored by the Department of Energy's Office of Biological and Environmental Research and located at Pacific Northwest National Laboratory. We thank Richard Kouzes for making arrangements for the ToF SIMS measurements. This work also benefited from our underground laboratory at the Waste Isolation Pilot Plant (WIPP), which we operate with support from the Nuclear Physics office of the U.S. Department of Energy under contract number 2011LANLE9BW. Finally, we thank our friends and hosts at the Waste Isolation Pilot Plant (WIPP) for their continuing support of our activities underground at that facility.

References

TABLE X: A summary of the uncertainties (in %) that contribute to the total uncertainty of cosmic production rate. The column labeled *SubTotal* refers to the quadrature sum of all non-cosmic-ray related contributions and provides the uncertainty for the ratio in Table IX.

Isotope (Line Energy)	Counting Statistics	Efficiency	Source Activity	Prediction from 4FP60R Fluence	Flux Chamber Live Time	SubTotal	Cosmic neutron flux	Proton Correction	Total
$^{57}\text{Co}(122)$	2.9	0.4	1.0	0.9	0.3	3.2	12.5	5.0	13.8
$^{57}\text{Co}(136)$	16.3	1.2	1.0	0.9	0.3	16.4	12.5	5.0	21.2
^{54}Mn	4.0	1.0	1.0	1.2	0.3	4.4	12.5	5.0	14.2
^{68}Ge	9.1	2.4	1.0	0.5	0.3	9.5	12.5	5.0	16.5
^{65}Zn	1.1	2.2	1.0	0.5	0.3	2.7	12.5	5.0	13.7
$^{60}\text{Co}(1173)$	3.0	3.0	1.0	0.6	0.3	4.5	12.5	5.0	14.2
$^{60}\text{Co}(1332)$	3.2	1.8	1.0	0.6	0.3	3.9	12.5	5.0	14.0

-
- [1] S. R. Elliott and P. Vogel, *Ann. Rev. Nucl. Part. Sci.* **52**, 115 (2002).
- [2] S. R. Elliott and J. Engel, *J. Phys. G: Nucl. Part. Phys.* **30**, R 183 (2004).
- [3] A. S. Barabash, F. Hubert, P. Huber, and V. I. Umatov, *Phys. At. Nucl.* **67**, 438 (2004).
- [4] F. T. III. Avignone, G. S. III. King, and Y. Zdesenko, *New Journal of Physics* **7**, 6 (2005).
- [5] H. Ejiri, *J. Phys. Soc. Jap.* **74**, 2101 (2005).
- [6] F. T. III. Avignone, S. R. Elliott, and J. Engel, *Rev. Mod. Phys.* **80**, 481 (2008), arXiv:0708.1033.
- [7] C. E. Aalseth et al. (IGEX), *Phys. Rev. D.* **65**, 092007 (2002).
- [8] L. Baudis et al., *Phys. Rev. Lett.* **83**, 41 (1999).
- [9] H. V. Klapdor-Kleingrothaus and I. V. Krivosheina, *Mod. Phys. Lett. A* **21**, 1547 (2006).
- [10] S. R. Elliott et al. (2008), arXiv:0807.1741.
- [11] V. E. Guiseppe et al. (2008), arXiv:0811.2446.
- [12] R. Henning et al. (2009), arXiv:0907.1581.
- [13] S. Schönert et al., *Nucl. Phys. Proc. Suppl.* **145**, 242 (2005).
- [14] H. S. Miley, F. T. Avignone, R. L. Brodzinski, W. K. Hensley, and J. H. Reeves, *Nucl. Phys. B (Proc. Suppl.)* **28A**, 212 (1992).
- [15] F. T. III. Avignone et al., *Nucl. Phys. B (Proc. Suppl.)* **28A**, 280 (1992).
- [16] S. Cebrián et al., *Journal of Physics: Conference Series* **39**, 344 (2006), TAUP 2005: Proc. Ninth Int. Conf. on Topics in Astroparticle and Underground Physics.
- [17] T. Horiguchi et al., *Int. J. Appl. Rad. Isot.* **34**, 1531 (1983).
- [18] Y. V. Aleksandrov et al., *Bull. Russ. Acad. Sci. - Phys. Ser.* **59**, 895 (1995).
- [19] E. B. Norman et al., *Nucl. Phys. B (Proc. Suppl.)* **143**, 508 (2005).
- [20] I. Barabanov, S. Belogurov, L. Bezrukov, A. Denisov, V. Kornoukhov, and N. Sobolevsky, *Nucl. Instrum. Meth. B* **251**, 115120 (2006).
- [21] D.-M. Mei, Z.-B. Yin, and S. R. Elliott, *Astropart. Phys.* **31**, 417420 (2009), arXiv:0903.2273.
- [22] J. J. Back and Y. A. Ramachers, *Nucl. Instrum. Meth. A* **586**, 286 (2008).
- [23] A. J. Koning, S. Hilaire, and M. C. Duijvestijn, in *Proceedings of the International Conference on Nuclear Data for Science and Technology - ND2004*, edited by R. C. Haight, M. B. Chadwick, T. Kawano, and P. Talou (2004), vol. 769, p. 1154.
- [24] J. F. Ziegler, *IBM J. Res. and Develop.* **42**, 117 (1998).
- [25] M. S. Gordon, P. Goldhagen, et al., *IEEE Transactions on Nuclear Science* **51**, 3427 (2004).
- [26] H. V. Klapdor-Kleingrothaus et al., *Nucl. Instrum. Meth. A* **481**, 149 (2002).
- [27] P. W. Lisowski, C. D. Bowman, G. J. Russell, and S. A. Wender, *Nucl. Sci. Eng.* **106**, 208 (1990).
- [28] J. A. Becker and R. O. Nelson, *Nucl. Phys. News* **7**, 11 (1997).
- [29] K. K. Gudima, S. G. Mashnik, and V. D. Toneev, *Nucl. Phys. A* **401**, 329 (1983).
- [30] S. G. Mashnik, M. I. Baznat, K. K. Gudima, A. J. Sierk, and R. E. Prael, *J. Nucl. Radiochem. Sci.* **6**, A1 (2005), nucl-th/0503061.
- [31] S. G. Mashnik, K. K. Gudima, R. E. Prael, A. J. Sierk, M. I. Baznat, and N. V. Mokhov, in *Invited lectures presented at the Joint ICTP-IAEA Advanced Workshop on Model Codes for Spallation Reactions* (2008), p. 51, LA-UR-08-2931, Los Alamos (2008); IAEA Report INDC(NDS)-0530, Distr. SC, Vienna, Austria, August 2008, arXiv:0805.0751v2 [nucl-th].
- [32] Yu. E. Titarenko et al., *Phys. Rev. C* **78**, 034615 (2008).